Inorganic Chemistry

pubs.acs.org/IC

Article

Solution Dynamics of Hybrid Anderson–Evans Polyoxometalates

David E. Salazar Marcano, Sarah Lentink, Mhamad A. Moussawi, and Tatjana N. Parac-Vogt*

Cite This: https://doi.org/10.1021/acs.inorgchem.1c00511

Read Online

ACCESS | Metrics & More | Article Recommendations | Supporting Information

ABSTRACT: Understanding the stability and speciation of metal-oxo clusters in solution is essential for many of their applications in different areas. In particular, hybrid organic–inorganic polyoxometalates (HPOMs) have been attracting increasing attention as they combine the complementary properties of organic ligands and metal–oxygen nanoclusters. Nevertheless, the speciation and solution behavior of HPOMs have been scarcely investigated. Hence, in this work, a series of HPOMs based on the archetypical Anderson–Evans structure, δ-$[MnMo_6O_{18}\{(OCH_2)_3C{-}R\}_2]^{3-}$, with different functional groups (R = $-NH_2$, $-CH_3$, $-NHCOCH_2Cl$, $-N{=}CH(2\text{-}C_5H_4N)$ {pyridine; −Pyr}, and $-NHCOC_9H_{15}N_2OS$ {biotin; −Biot}) and countercations (tetrabutylammonium {TBA}, Li, Na, and K) were synthesized, and their solution behavior was studied in detail. In aqueous solutions, decomposition of HPOMs into the free organic ligand, $[MoO_4]^{2-}$, and free Mn^{3+} was observed over time and was shown to be highly dependent on the pH, temperature, and nature of the ligand functional group but largely independent of ionic strength or the nature of the countercation. Furthermore, hydrolysis of the amide and imine bonds often present in postfunctionalized HPOMs was also observed. Hence, HPOMs were shown to exhibit highly dynamic behavior in solution, which needs to be carefully considered when designing HPOMs, particularly for biological applications.

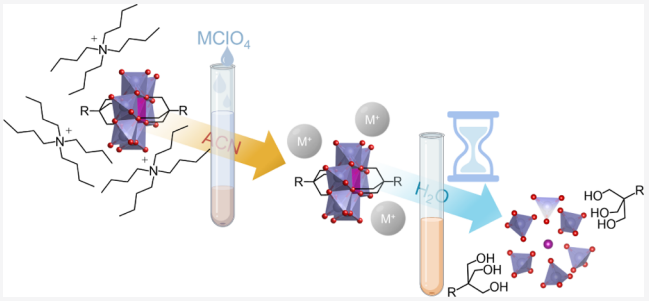

INTRODUCTION

Polyoxometalates (POMs) are a large class of anionic metal–oxygen clusters with highly tunable physical and chemical properties, which can be made even more versatile by functionalization with organic moieties. All-inorganic POMs of different shapes, sizes, nuclearities, and charge densities are well known to form by self-condensation of metal-oxo anions of certain metals in their highest oxidation states (commonly W^{6+}, Mo^{6+}, and V^{5+}) depending on the pH, concentration, and ionic strength.[1] These structures are highly adaptable, and other elements can be incorporated either at lacunary sites or as templates around which the POM can form.[2,3] Organic molecules can also be covalently attached to the inorganic core to form organic–inorganic hybrid polyoxometalates (HPOMs) that benefit from the synergistic properties of both the organic and inorganic components. Hence, the hybrid nature of HPOMs allows for the development of a new family of compounds with an extended range of applications in catalysis, materials science, and medicine.[4−7]

Functionalization of POMs opens up many possibilities in POM chemistry. Structures that are yet to be obtained as stand-alone anions, such as the commonly studied manganese hexamolybdate Anderson–Evans ($[MnMo_6O_{24}]^{9-}$, AE) and the hexavanadate Lindqvist ($[V_6O_{19}]^{8-}$) structures, can be accessed through functionalization by forming the corresponding HPOMs (e.g., $[MnMo_6O_{18}\{(OCH_2)_3C{-}R\}_2]^{3-}$ and $[V_6O_{13}\{(OCH_2)_3C{-}R\}_2]^{2-}$; R = organic moiety).[2,8] The organic ligand grafted onto the POM can also be used as a linker for covalent attachment of POMs on surfaces,[9] nanoparticles,[10] polymers,[11] and even onto other clusters[12−14] among many possibilities. In addition, HPOMs can form supramolecular structures such as micelles,[15] vesicles,[16,17] and extended structures.[18−20] Moreover, enhanced properties may be achieved through the combination of POMs with organic compounds, such as a greater photocoloration contrast obtained with spyropiran-POM hybrids.[21,22] Grafting organic ligands onto POMs can also reduce their toxicity and increase their lipophilicity, which is interesting for their use as protein crystallization agents or in other biological applications since POMs are known to have potential as antitumor, antiviral, and antibacterial drugs.[23−25] Therefore, the synergy of the organic and inorganic components of HPOMs can be highly beneficial.

Out of the many POMs that have been functionalized so far, the archetypical AE structure with the general formula $[\{X^{n+}O_6\}M_6O_{18}]^{(12-n)-}$ (M = Mo^{6+} or W^{6+}; X = heteroatom) is particularly interesting since it offers a highly adaptable platform that can be easily tailored to the desired purposes,

Received: February 18, 2021

and therefore, it is one of the most commonly reported HPOM structures (Figure 1).[2,6] The inorganic core is composed of six

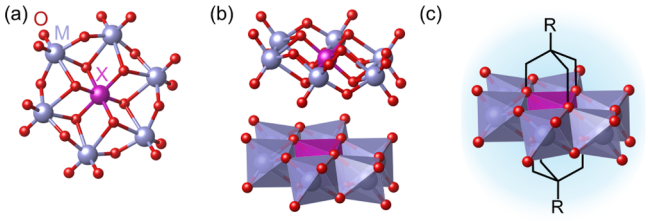

Figure 1. Representations of the AE structure $[\{X^{n+}O_6\}M_6O_{18}]^{(12-n)-}$ (a) top and (b) side view, as well as (c) the most common isomer of the tris(alkoxo) functionalized AE POMs δ-$[\{X^{n+}O_6\}M_6O_{12}\{(OCH_2)_3C{-}R\}_2]^{(6-n)-}$. Oxygen in red, metal addenda atom M (W or Mo) in purple, heteroatom X in magenta, and organic carbon chain in the skeletal form in black.

edge-sharing $\{MO_6\}$ octahedra which can accommodate a wide variety of central heteroatoms in different oxidation states, including most first-row transition metals and even some p-block elements (e.g., X = Cr, Mn, Fe, Co, Ni, Cu, Zn, Ga, Al, Te, etc.), thereby tuning the electronic and magnetic properties of the structure.[2] The AE structure can also be grafted with many different types of organic molecules, which is generally achieved by replacing some of the oxo ligands (formally O^{2-}) with tris(alkoxo) ligands ($(OCH_2)_3C{-}R$). Moreover, HPOMs can be further postfunctionalized by many different synthetic pathways[6,26] including amidation,[27] nucleophilic substitution,[28] and click chemistry,[29] depending on the nature of the functional group (e.g., R = $-NH_2$, $-NHCOCH_2Cl$, $-NHCOCH_2N_3$, etc.). Hence, the large diversity and tailorability of AE HPOMs have attracted significant interest in recent years, and among the many reported structures, the bis-functionalized manganese hexamolybdate δ-$[MnMo_6O_{18}\{(OCH_2)_3C{-}R\}_2]^{3-}$ (denoted herein as AE−R) has been the most commonly investigated (Figure 1c).[2,6]

Like many functionalized POMs, the AE−R HPOMs are often synthesized as tetrabutylammonium (TBA) salts that dissolve in polar organic solvents but are poorly soluble in water, which limits their applications in water-based catalytic and biological systems.[30−32] Nevertheless, the solubility of HPOMs can be tuned by exchanging TBA for alkali metal countercations, thereby adding further versatility to the system.[33] Such an exchange is sometimes achieved using an ion-exchange resin, but the Na salts can also be more easily and quickly obtained by precipitation through the addition of sodium perchlorate.[20,34,35] However, the latter method and the effect of changing the counterion on the solubility of HPOMs in different solvents has been less commonly systematically investigated and reported, especially for metal countercations other than sodium. Moreover, as the high versatility of POMs makes them highly attractive compounds, it is essential to understand their solution speciation and stability over time in order to obtain the desired structures and to determine the nature of the active species, particularly in catalytic and medicinal applications.[36,37] As a result, the speciation of all-inorganic POMs in water has been extensively investigated, as described in a recent excellent review by Gumerova and Rompel.[38] However, despite the large potential of HPOMs, their speciation and solution dynamics have been very rarely explored.

Although functionalization of POMs is generally expected to enhance their stability, reports on the actual stability of HPOMs in different solvents remain relatively scarce. Electrospray ionization mass spectrometry (ESI-MS) has been used to investigate the formation process of AE−R HPOMs during synthesis, and this technique has also been used to determine the stability of $GaMo_6$, $FeMo_6$, and $MnMo_6$ AE−R HPOMs, which appear to be hydrolytically stable over 24 h in buffered aqueous solutions at different pH values.[34,39,40] However, a molecular understanding of the solution stability of HPOMs over longer periods of time, as well as the factors that influence their speciation, is still largely lacking. Understanding the stability of these HPOMs in water is particularly important in the context of their promising potential in aiding protein crystallization, as this process involves placing the HPOM in aqueous solution with a protein for several days, while single crystals suitable for X-ray diffraction gradually form.[41] Furthermore, the potential biomedical applications of HPOMs as drugs make it essential for their solution dynamics

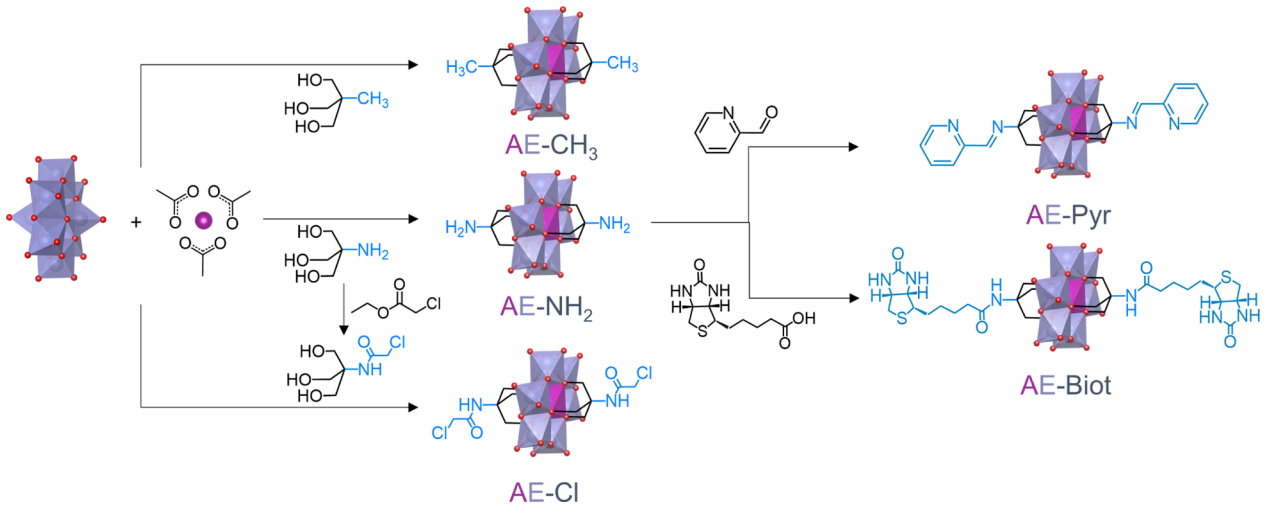

Figure 2. Synthesis of δ-$[MnMo_6O_{18}\{(OCH_2)_3C{-}R\}_2]^{3-}$ (AE−R) HPOMs with different functional groups from α-octamolybdate ($TBA_4[\alpha$-$Mo_8O_{26}]$), manganese (III) acetate, and the corresponding triol ligand ($(HOCH_2)_3C{-}R$) in an organic solvent by direct, pre-, and postfunctionalization.

https://doi.org/10.1021/acs.inorgchem.1c00511
Inorg. Chem. XXXX, XXX, XXX−XXX

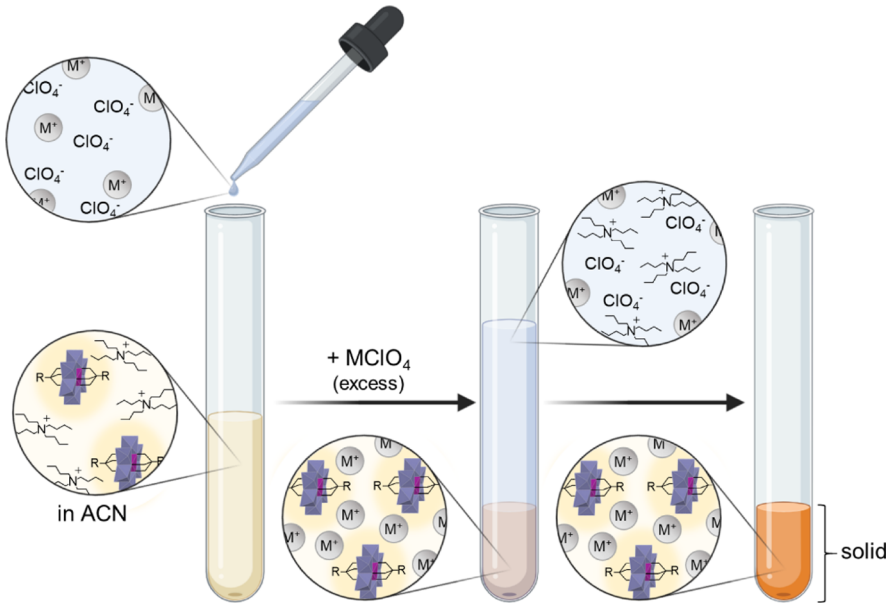

Figure 3. Cation metathesis for obtaining water-soluble M−AE−R HPOMs by precipitation from a saturated solution of the TBA salt via addition of the metal perchlorate (M = Li, Na, or K).

to be thoroughly investigated.[23,24,42] Therefore, in this study, the solution behavior of a range of AE−R HPOMs with different countercations and functional groups was thoroughly investigated in different solvents and under different conditions by nuclear magnetic resonance (NMR) and ultraviolet−visible (UV−vis) spectroscopy. The systematic approach used in this study allowed us to provide a detailed account of the effect of the HPOM structure (i.e., countercation and functional group) and solution conditions (i.e., solvent, concentration, ionic strength, pH, and temperature) on the stability and speciation of AE−R HPOMs in solution from a few minutes after dissolution up to several weeks later.

RESULTS AND DISCUSSION

A solution stability and speciation study was performed on a series of HPOMs, shown in Figure 2, which were chosen due to their complementary structure and properties. This series involved the following AE−R HPOMs: δ-$[MnMo_6O_{18}\{(OCH_2)_3C-NH_2\}_2]^{3-}$ (**AE−NH$_2$**), δ-$[MnMo_6O_{18}\{(OCH_2)_3C-CH_3\}_2]^{3-}$ (**AE−CH$_3$**), δ-$[MnMo_6O_{18}\{(OCH_2)_3C-NHCOCH_2Cl\}_2]^{3-}$ (**AE−Cl**), δ-$[MnMo_6O_{18}\{(OCH_2)_3C-N{=}CH(2\text{-}C_5H_4N)\}_2]^{3-}$ (**AE−Pyr**), and δ-$[MnMo_6O_{18}\{(OCH_2)_3CNHCOC_9H_{15}N_2OS\}_2]^{3-}$ (**AE−Biot**). These HPOMs have the same **MnMo$_6$** core but vary in the nature of functional groups present in the organic ligands. **AE−NH$_2$** can form H-bonds and can additionally serve as a platform for postfunctionalization by imine or amide bond formation. Such a postfunctionalization yields the aromatic **AE−Pyr**, functionalized with pyridine (Pyr), and the biologically relevant **AE−Biot**, functionalized with biotin (Biot), an essential vitamin that also has one of the strongest known interactions with its binding proteins.[27,43] Furthermore, **AE−Cl**, synthesized by prefunctionalization of tris(hydroxymethyl)-aminomethane ($(HOCH_2)_3CNH_2$), has both polar and H-bonding functional groups and has been shown to serve as an excellent platform for further postfunctionalization with amines, carboxylic acids, and thiols by nucleophilic substitution or with alkynes by copper-catalyzed azide−alkyne cycloaddition upon replacement of the chlorines with azides.[28,29] In contrast, **AE−CH$_3$**, one of the first reported AE HPOMs, has a similar size and molecular weight to **AE−NH$_2$** but has a nonpolar hydrophobic methyl group instead.[44] Overall, these HPOMs cover a broad range of possible functional groups and therefore allow for a comprehensive study of the dynamics of HPOMs in solution.

Tuning the Solubility via Cation Metathesis. The solubility of POMs, in general, highly depends on the nature of the countercation.[33] The as-synthesized TBA salts of the AE−R HPOMs were found to be highly soluble in polar aprotic solvents and less soluble in polar protic solvents (Table S1). Their solubility was the highest in dimethyl sulfoxide (DMSO), with a solubility greater than 100 mg/mL for all HPOMs. The solubility in acetonitrile (ACN), which has a lower dielectric constant, varied between 9 and 200 mg/mL depending on the functionalization: **AE−NH$_2$** had the highest solubility (200 mg/mL) due to its short and polar amine group, while the solubility of **AE−CH$_3$** (83 mg/mL) was more than twice lower due to the presence of nonpolar methyl groups. Further lengthening of the functional group resulted in lower solubility, as observed for **AE−Cl** (43 mg/mL) and **AE−Biot** (27 mg/mL), while **AE−Pyr** was even less soluble (9 mg/mL) due to the highly hydrophobic aromatic group. In methanol (MeOH), the HPOMs were significantly less soluble with only **AE−NH$_2$** (110 mg/mL) and **AE−CH$_3$** (21 mg/mL) having solubilities higher than 1 mg/mL. On the other hand, in water, for all HPOMs, the solubility was less than 5 mg/mL. Hence, in order to modify the solubility of AE−R HPOMs and especially to increase their solubility in water, TBA was exchanged for Li^+, Na^+, and K^+ by a cation metathesis procedure involving precipitation of the alkali metal salt. This procedure was optimized in order to obtain 100% conversion of the TBA salts into the alkali metal salts within minutes and in high yields while using a minimal amount of solvent, thereby easily expanding the repertoire of possible HPOM countercations to different alkali metals (Figure 3).

This cation metathesis procedure consisted of adding a saturated solution of the metal perchlorate in excess to a saturated solution of the TBA salt in ACN, resulting in instant

https://doi.org/10.1021/acs.inorgchem.1c00511
Inorg. Chem. XXXX, XXX, XXX−XXX

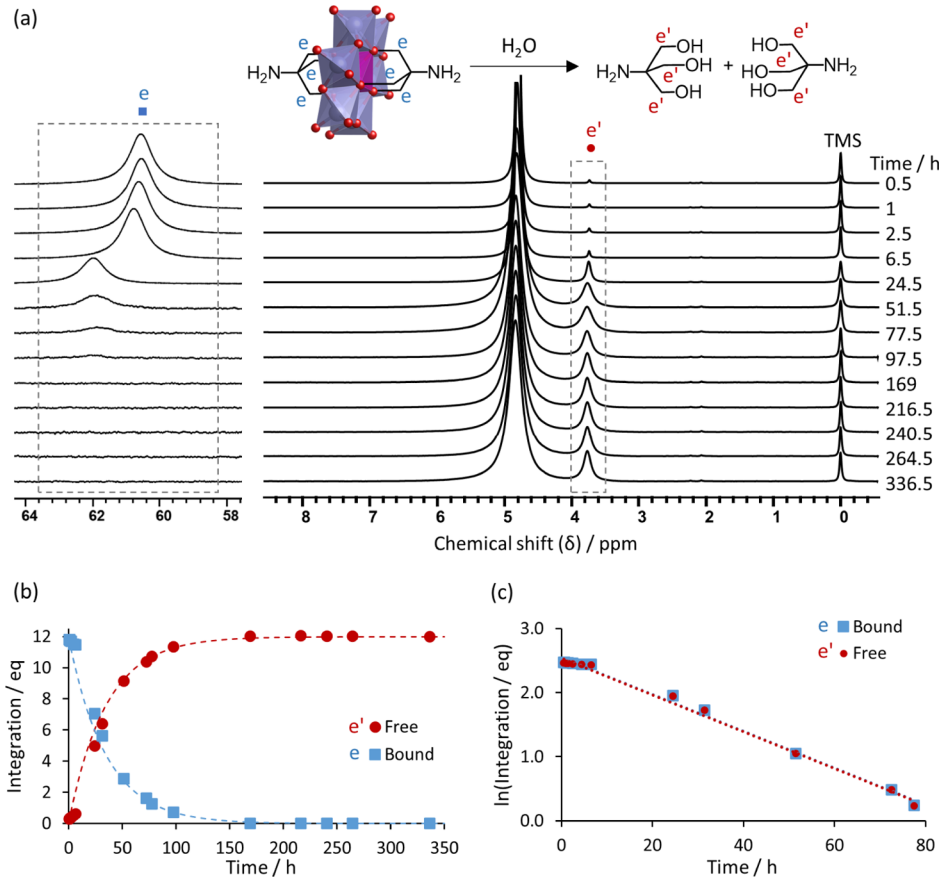

Figure 4. (a) ^{1}H NMR spectra of 5 mg/mL Na−AE−NH_2 in D_2O at pD 7.3 acquired over 340 h at room temperature, displaying a decrease in the integration of the peak due to the POM-bound $-OCH_2-$ protons and a matching increase in the integration of the peak due to the $-OCH_2-$ protons of the free ligand resulting from the decomposition reaction shown above. (b) Plot of the relative integration of the peaks in proton equivalents over time and the corresponding exponential curves for a pseudo-first-order reaction using the observed rate constant (k_{obs}) obtained from plot (c): 8.0 ± 0.4 × 10^{-6} s^{-1} (R^2 = 0.994).

precipitation of the metal salt of the HPOM, while residual metal perchlorate and TBA perchlorate remained in solution. This was confirmed by ^{1}H NMR and ESI-MS analysis of the supernatant, which showed only the characteristic peaks of TBA and perchlorate with no indication of the HPOM being present. The precipitate was then washed multiple times with ACN to remove any remaining perchlorate and TBA. The washes were also followed by ESI-MS and showed that the perchlorate peaks gradually disappeared. The precipitate was then vacuum-dried at 50 °C. Complete conversion to the metal salt and removal of all TBA from the HPOMs were then confirmed by IR and NMR spectroscopy. The bands in the IR spectrum due to C−H stretching and bending vibrations of TBA at 2800−3000 and 1480 cm^{-1} decreased in intensity after the cation metathesis, while the fingerprint of the POM core with peaks due to vibrations of Mo═O and Mo−O−Mo bonds remained intact (Figures S1−S5). The typical ^{1}H NMR resonances of TBA were also absent in the spectrum after the cation metathesis (Figures S9−S13).

The alkali metal salts (M-HPOMs) were water-soluble (>200 mg/mL for Li- and Na-HPOMs), but as expected, the K-HPOMs were the least soluble (<20 mg/mL) and all were poorly soluble in ACN (<1 mg/mL). However, although the Li salts were very poorly soluble in ACN, they were highly soluble in DMSO (>200 mg/mL) and the solubility in MeOH was even higher than for the TBA salts, except for **AE−NH_2**. On the other hand, the Na- and K-HPOMs were very poorly soluble in MeOH (<1 mg/mL), and their solubility in DMSO was lower than that of the Li-HPOMs (<70 mg/mL for Na-HPOMs and <7 mg/mL for K-HPOMs). In fact, the solubility of **K-AE−Pyr** was so low that it could not be successfully characterized and was therefore excluded from the study. Hence, for applications where high solubility in a variety of media is required, such as homogeneous catalysis, the Li salts would be the most suitable choice. However, if a lower solubility is preferred, as is the case in crystallography, the use of K-HPOMs would be better suited, while the Na-HPOMs can be used when a more intermediate solubility is desired.

Stability in Water. Once water-soluble AE−R HPOMs were obtained, their stability in aqueous conditions was monitored over time. The stability of AE−R HPOMs can be conveniently followed by ^{1}H NMR since the Mn^{3+} central heteroatom causes significant paramagnetic deshielding of neighboring protons. In particular, the twelve $-OCH_2-$ protons in the tripodal anchor of the tris(alkoxo) ligand ($[MnMo_6O_{18}\{(\mathbf{OCH_2})_3C-R\}_2]^{3-}$) give rise to a broad peak at a high chemical shift of around 50−70 ppm when bound to the POM core.[28,29,44] In contrast, the ^{1}H NMR resonances of the free protonated ligand ($(\mathbf{HOCH_2})_3C-R$) occur at a chemical shift of 3.5−4.0 ppm (depending on the nature of the R group). Hence, decomposition of AE−R HPOMs, which over time leads to the formation of the free ligand, can be followed by the increase in a peak at 3.5−4.0 ppm in the ^{1}H NMR spectra and a corresponding decrease in the peak at 50−70

https://doi.org/10.1021/acs.inorgchem.1c00511
Inorg. Chem. XXXX, XXX, XXX−XXX

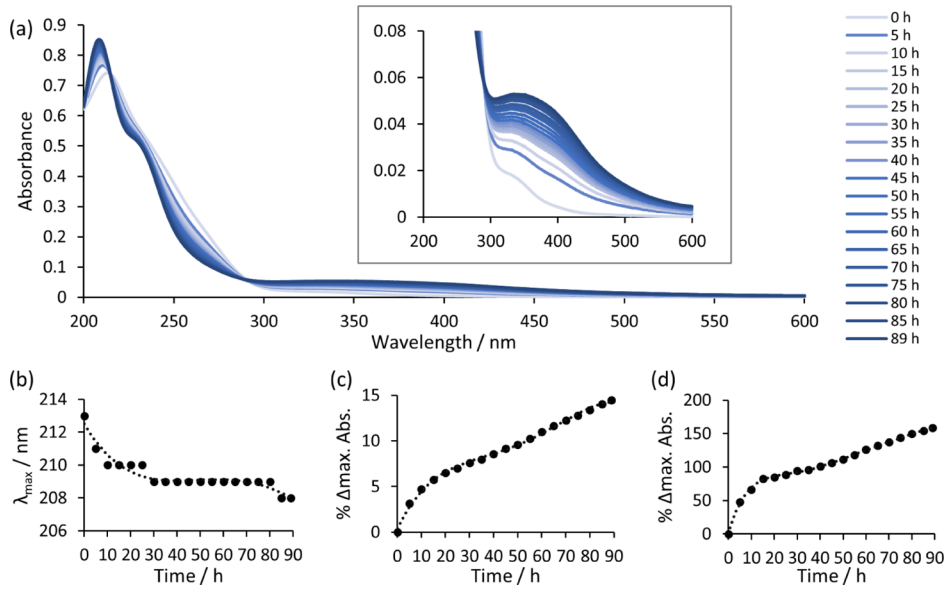

Figure 5. (a) UV−vis spectra of 0.02 mg/mL Li−AE−NH_2 in water at pH 7 acquired over 89 h at room temperature with the weaker peak at 300−400 nm due to the d−d transition of Mn^{3+} shown in more detail in the inset. Plots of (b) the change over time in λ_{max} and of the percentage change in maximum absorbance (c) from 200 to 600 nm, corresponding to the LMCT of Mo−O, and (d) from 300 to 600 nm, corresponding to the d−d transition of Mn^{3+}.

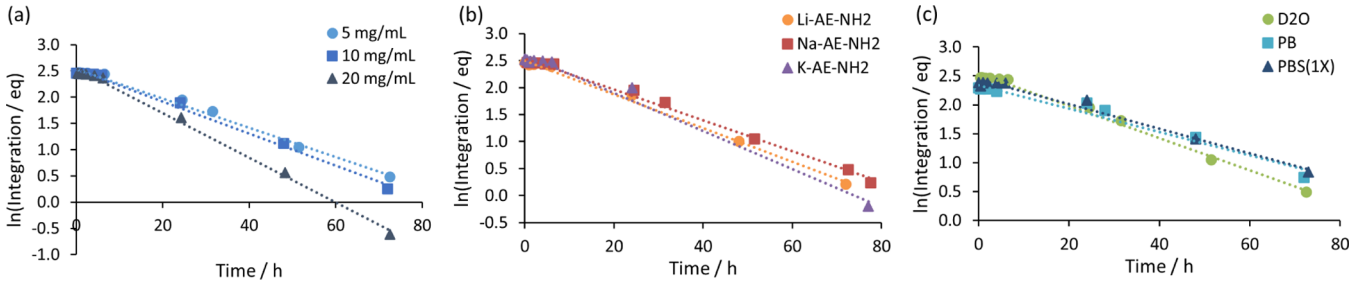

Figure 6. Plot of ln(integration) against time for the integration of the peak due to the bound $-OCH_2-$ protons of Na-AE−NH_2 in D_2O at pD 7.3 (5 mg/mL; I = 0.0246 M; k_{obs} = 8.0 ± 0.4 × 10^{-6} s^{-1}; R^2 = 0.994) together with the corresponding data for (a) 10 and 20 mg/mL Na−AE−NH_2 in D_2O, from which k_{obs} values were determined to be 8.5 ± 0.6 × 10^{-6} s^{-1} (R^2 = 0.993) and 11.8 ± 0.7 × 10^{-6} s^{-1} (R^2 = 0.996), respectively, (b) Li- and K−AE−NH_2 in D_2O (5 mg/mL), from which k_{obs} values were determined to be 9.0 ± 0.6 × 10^{-6} s^{-1} (R^2 = 0.995) and 9.1 ± 1.2 × 10^{-6} s^{-1} (R^2 = 0.985), respectively, and (c) 5 mg/mL Na−AE−NH_2 in PB at pD 7.4 (I = 0.0564) and in PBS(1×) at pD 7.4 (I = 0.1961 M), from which k_{obs} values were determined to be 5.6 ± 1.0 × 10^{-6} s^{-1} (R^2 = 0.965) and 5.9 ± 0.7 × 10^{-6} s^{-1} (R^2 = 0.982), respectively.

ppm. This was most clearly observed for a solution of **Na−AE−NH_2** in D_2O over a period of 14 days (Figure 4), and a similar trend was seen for all other HPOMs in this study (Figures 11; S15−S18).

Following changes over time in the integration of the peaks due to the bound and free $-OCH_2-$ protons showed that **Na−AE−NH_2** in D_2O at pD 7.3 decomposed by almost 41% after 24 h and by 94% after 97.5 h (Figure 4). This corresponds to a 94% decrease in the integration of the peak due to the POM-bound ligand and a matching 94% increase in the integration of the peak due to the free ligand after 97.5 h, indicating that the HPOM almost completely dissociated in 4 days. The decomposition of **Na−AE−NH_2** in D_2O followed a pseudo-first-order kinetic rate law with an observed rate constant (k_{obs}) of 8.0 ± 0.4 ×10^{-6} s^{-1}. This rate constant was determined by following changes in the integration of the peaks corresponding to the bound and free $-OCH_2-$ groups (Figure 4c), based on the total amount of ligand remaining the same in solution ([AE−R] = $[AE-R]_0$ − [Tris−R], where [AE−R] is the concentration of the HPOM, $[AE-R]_0$ is the initial concentration of the HPOM, and [Tris−R] is the concentration of the free ligand), both of which showed the same kinetics during the first 77 h.

Decomposition of **AE−NH_2** in ultrapure water was also observed by UV−vis spectroscopy (Figure 5). The AE structure gives rise to a distinctive peak in the UV−vis absorbance spectrum in the region of 200−220 nm due to the ligand to metal charge transfer (LMCT) transition from the ligand-centered μ_3-OR π orbitals to the metal-centered Mo^{6+} t_{2g} orbitals, and the position of the maximum absorbance (λ_{max}) of this peak depends on the nature of the ligand.[12,45,46] In addition, a much weaker and broader band in the visible region, around 300−400 nm, is present due to the d−d transition of the HOMO t_{2g} to the LUMO e_g of Mn^{3+}. Both of these peaks were observed to change over time for a solution of **Li−AE−NH_2** in water. The position of λ_{max} blue-shifted from 213 nm toward 208 nm, and a shoulder peak appeared at around 230 nm (Figure 5b). These changes in the UV−vis absorbance spectrum correspond to the formation of the molybdate ion ($[MoO_4]^{2-}$), indicating that the AE POM structure decomposed into its basic building blocks.[47] The absorbance of the dominant peak at 208 nm also increased

https://doi.org/10.1021/acs.inorgchem.1c00511
Inorg. Chem. XXXX, XXX, XXX−XXX

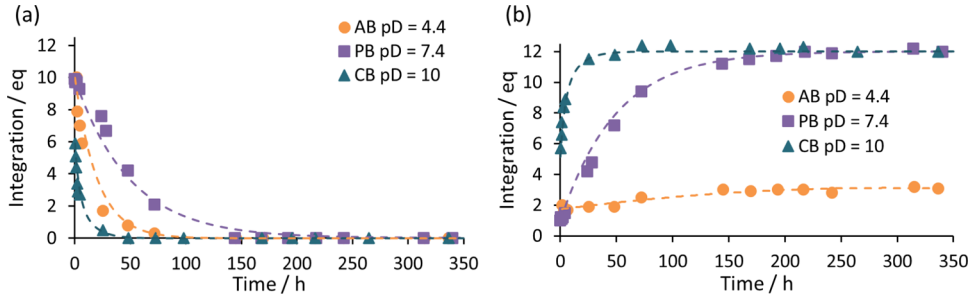

Figure 7. Plots of the relative integration over time of the (a) peak due to the POM-bound $-OCH_2-$ protons and (b) peak due to the $-OCH_2-$ protons in the free ligand for 5 mg/mL solutions of Na−AE−NH_2 in AB at pD 4.4, PB at pD 7.4, and CB at pD 10.

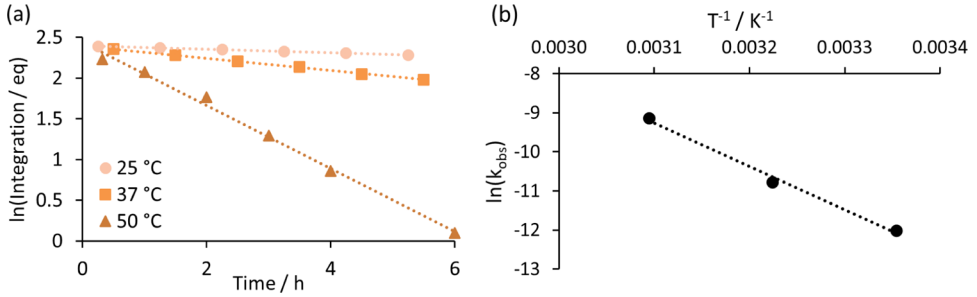

Figure 8. (a) Plot of ln(integration) against time for the pseudo-first-order decomposition reaction of 5 mg/mL Li−AE−NH_2 in deuterated PBS(1×) at 25 °C with a k_{obs} of 6.1 ± 1.2 × 10^{-6} s^{-1} (R^2 = 0.995), 37 °C with a k_{obs} of 20.8 ± 1.7 × 10^{-6} s^{-1} (R^2 = 0.999), and 50 °C with a k_{obs} of 107.5 ± 17.1 × 10^{-6} s^{-1} (R^2 = 0.994) and (b) the corresponding Arrhenius plot of ln(k_{obs}) as a function of T^{-1} with an E_a of 92 kJ mol^{-1} (R^2 = 0.993).

over time as the concentration of $[MoO_4]^{2-}$ gradually increased (Figure 5c). In addition, the peak around 300−400 nm due to the d−d transition of Mn^{3+} was also observed to increase over time, indicating a change in the coordination environment of Mn^{3+} (Figure 5d). Overall, both UV−vis and ^{1}H NMR show gradual changes over several hours in the spectra of HPOMs in aqueous solutions that are clearly due to the decomposition of the POM core into $[MoO_4]^{2-}$ and Mn^{3+} as the ligand is released into solution.

Influence of Concentration and the Presence of Ions in Solution. The influence of the composition of the solution—such as HPOM concentration, the counterion, ionic strength, and pH—on the stability of AE−R HPOMs was also investigated. Increasing the concentration of **Na−AE−NH_2** in D_2O resulted only in a slight increase in the rate of decomposition as can be seen from the k_{obs} obtained for 5 mg/mL (4 mM), 10 mg/mL (8 mM), and 20 mg/mL (16 mM) solutions: 8.0 ± 0.4 × 10^{-6}, 8.5 ± 0.6 × 10^{-6}, and 11.8 ± 0.7 × 10^{-6} s^{-1}, respectively, as determined from changes in the integration of the $-OCH_2-$ peaks in the ^{1}H NMR spectra based on pseudo-first-order kinetics (Figures 6a; S14). Similarly, although the counterion has a significant effect on the solubility, it did not show any noticeable effect on the rate of decomposition, suggesting that solubility can be tuned without affecting stability (Figures 6b; S15). As a result, the Li-, Na-, and K-HPOMs dissolved in D_2O decomposed with highly comparable k_{obs}, which were in the range of 8 × 10^{-6} to 9 × 10^{-6} s^{-1}. Moreover, increasing the ionic strength through the presence of additional ions in solution had little effect on the stability of the HPOMs. Hence, **AE−NH_2** decomposed at approximately the same rate in D_2O at pD 7.3, in deuterated phosphate buffer (PB) at pD 7.4, composed of 10 mM Na_2HPO_4 and 1.8 mM KH_2PO_4, and in deuterated phosphate-buffered saline (PBS(1×)) at pD 7.4, which is meant to simulate physiological conditions and was therefore composed of 10 mM Na_2HPO_4, 1.8 mM KH_2PO_4, 2.7 mM KCl, and 137 mM NaCl (Figures 6c; S19−S22). This indicates that ions in solution do not play a role in the decomposition of AE−R HPOMs since the much higher salt content of PBS(1×), which resulted in an ionic strength of 0.1961 M for the HPOM solution, gave a similar k_{obs} to solutions in PB and in D_2O, which had lower ionic strengths by ca. 3.5 and 8 times, respectively.

Influence of pH and Temperature. Following the HPOMs in deuterated buffered solutions at pD 4.4, 7.4, and 10.0 clearly showed that the pD had a significant effect on the rate of their decomposition in aqueous solutions (Figures 7; S21−S26). For **AE−NH_2** in deuterated carbonate buffer (CB) at pD 10.0, more than 50% decomposition occurred within the first 30 min and essentially full decomposition was observed after 24 h, showing a much faster decomposition rate due to the high pD when compared to PB at pD 7.4, in which **AE−NH_2** only decomposed by 35% after 24 h. A dark brown precipitate was also observed to form after a few hours, which most likely corresponds to a manganese (III) salt precipitating out of solution since the IR spectrum of the precipitate did not display the characteristic bands of the POM core and a similar spectrum was obtained for the precipitate formed from manganese (III) acetate in CB (Figure S6). In deuterated acetate buffer (AB) at pD 4.4, precipitation was also observed over time, but in this case, it was due to the protonation of **AE−NH_2**, which reduces its net charge, making it less soluble, since the IR spectrum of the precipitate showed that the POM core remained intact, and a similar IR spectrum was obtained for the precipitate formed by adding 1 M HCl to a solution of **AE−NH_2** in water to lower the pH to 4.3 (Figure S7). This precipitation led to an observable decrease over time in the integration of the peak corresponding to the bound $-OCH_2-$

https://doi.org/10.1021/acs.inorgchem.1c00511
Inorg. Chem. XXXX, XXX, XXX−XXX

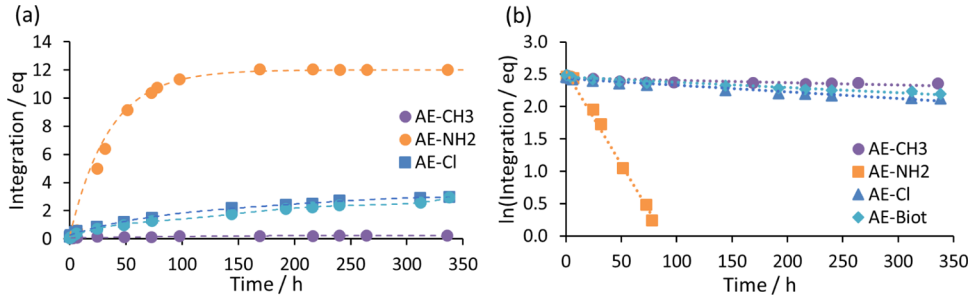

Figure 9. (a) Plot displaying changes in the integration over time of the peak due to the $-OCH_2-$ protons of the free ligand released by the decomposition of AE−R in D_2O (5 mg/mL) and (b) the corresponding plot of ln(integration) against time for the integration of the peak due to the bound $-OCH_2-$ protons, from which k_{obs} values were determined to be 0.10 ± 0.04 × 10^{-6} s^{-1} (R^2 = 0.723), 7.96 ± 0.44 × 10^{-6} s^{-1} (R^2 = 0.994), 0.29 ± 0.03 × 10^{-6} s^{-1} (R^2 = 0.965), and 0.28 ± 0.03 × 10^{-6} s^{-1} (R^2 = 0.954) for R = $-CH_3$, $-NH_2$, −Cl ($-NHCOCH_2Cl$), and −Biot (biotin) respectively.

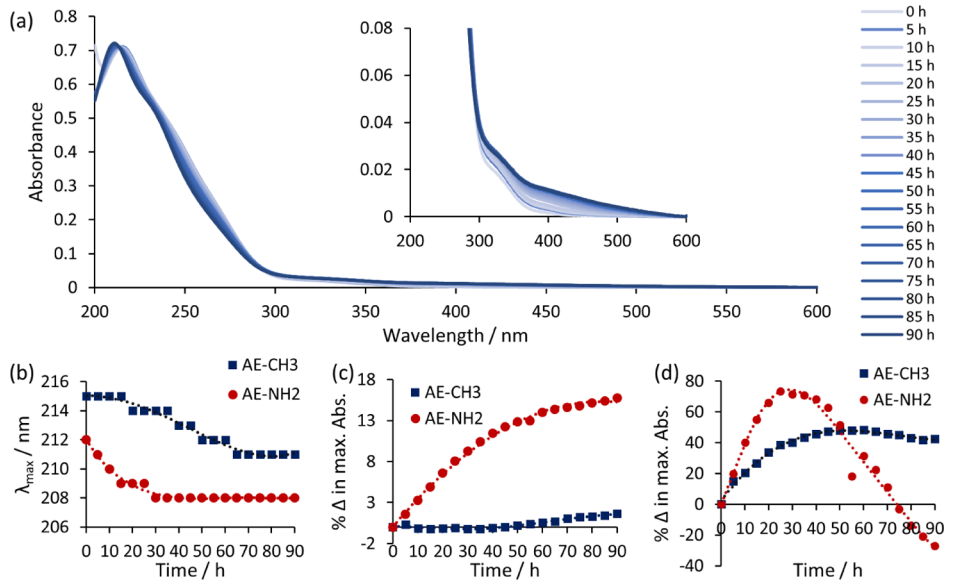

Figure 10. (a) UV−vis spectra of 0.02 mg/mL Li−AE−CH_3 in PBS(1×) at pH 7.4 acquired over 90 h at room temperature with the weaker peak at 300−400 nm due to the d−d transition of Mn^{3+} shown in more detail in the inset. Plots of (b) change over time in λ_{max} and of the percentage change in maximum absorbance (c) from 200 to 600 nm, corresponding to the LMCT of Mo−O, and (d) from 300 to 600 nm, corresponding to the d−d transition of Mn^{3+} for solutions of AE−CH_3 and AE−NH_2 in PBS(1×) at pH 7.4.

protons, which gradually disappeared (Figure 7a). However, a corresponding increase in the peak due to $-OCH_2-$ protons in the free ligand was not observed, despite the ligand being soluble in AB (Figure 7b). In fact, hardly any further changes in the ^1H NMR spectrum were observed over 14 days, indicating that little to no further decomposition took place. Furthermore, a solution of **AE−CH_3** in AB at pD 4.4 was also followed by ^1H NMR (Figure S24), and the peaks due to the bound $-OCH_2-$ and $-CH_3$ protons remained more or less unchanged during 14 days as **AE−CH_3** did not precipitate out of solution. Consequently, it can be concluded that HPOMs are most stable in aqueous solutions with lower pH.

It was also observed that the temperature of the solution has a notable effect on the decomposition of **AE−NH_2** in deuterated PBS(1×) at pD 7.4 (Figures 8; S27−S30). ^1H NMR spectra were acquired every hour over 6 h at exactly 25 °C, and at this temperature, k_{obs} was calculated to be 6.1 ± 1.2 × 10^{-6} s^{-1}, corresponding to the initial rate of decomposition. However, when the solution was placed at 37 °C, to more closely simulate physiological conditions, the value of k_{obs} more than tripled to 20.8 ± 1.7 × 10^{-6} s^{-1}. Increasing the temperature of the solution further by the same amount to 50 °C and following changes by ^1H NMR over 6 h gave a k_{obs} of 107.5 ± 17.1 × 10^{-6} s^{-1} (Figure 8a), almost 20 times higher than at 25 °C. From this temperature dependence of k_{obs}, the activation energy of dissociation was estimated using the Arrhenius equation to be around 92 kJ mol^{-1} (Figure 8b). Once this kinetic barrier is overcome, there is a clear entropic gain in decomposition as multiple separate molecules are formed from each HPOM.

Influence of the Functional Group. Interestingly, the nature of the organic functional group of the AE−R HPOMs had a notable effect on the stability of the HPOMs in D_2O (Figures 9; S14−S18). **AE−NH_2** decomposed much faster than all the other HPOMs in this study. Full decomposition was observed after 98 h for **AE−NH_2**, while **AE−CH_3** remained relatively stable even after 336 h in D_2O and showed the slowest rate of decomposition (k_{obs} = 0.1 ± 0.04 × 10^{-6} s^{-1}). The HPOMs with amide-bound moieties, **AE−Cl** (k_{obs} = 0.3 ± 0.03 × 10^{-6} s^{-1}) and **AE−Biot** (k_{obs} = 0.2 ± 0.02 × 10^{-6} s^{-1}), displayed very similar intermediate stability as only around 25% decomposition was observed after 338 h.

https://doi.org/10.1021/acs.inorgchem.1c00511
Inorg. Chem. XXXX, XXX, XXX−XXX

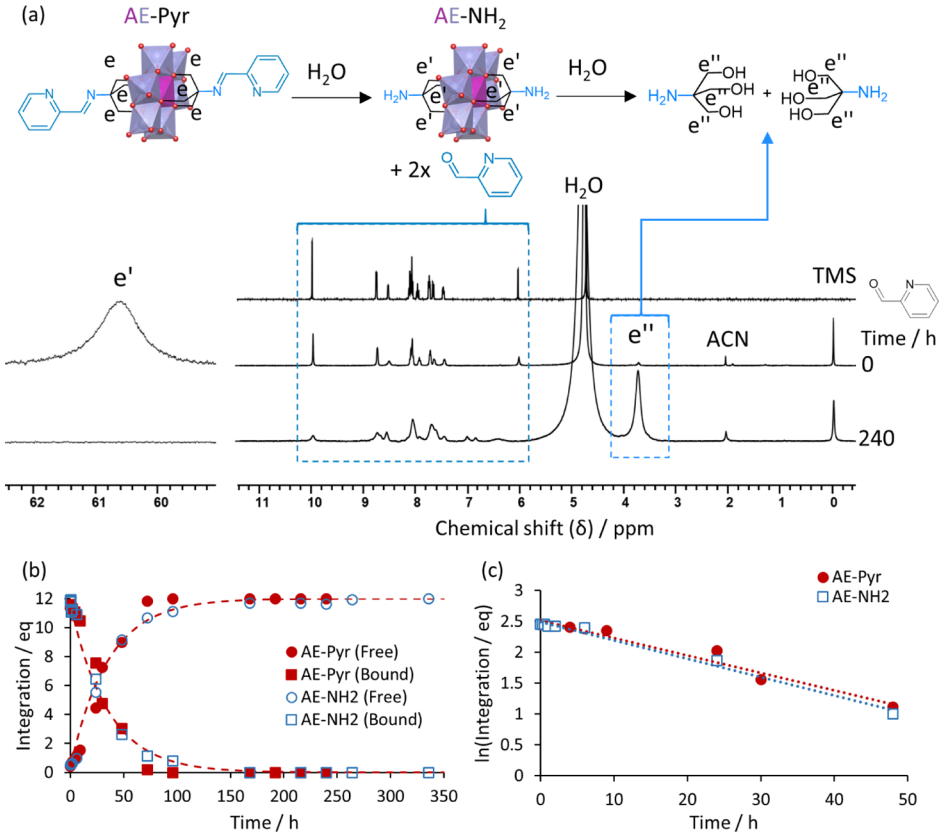

Figure 11. (a) Decomposition of AE−Pyr in D_2O (5 mg/mL) resulting in hydrolysis of the ligand and the HPOM as shown by the ^1H NMR spectra of pyridinecarbaldehyde and of AE−Pyr after 0 and 240 h in D_2O. (b) Plot of the relative integration in proton equivalents over time of the peaks due to the $-OCH_2-$ protons of AE−Pyr and AE−NH_2 in D_2O and the corresponding exponential curves for a pseudo-first-order reaction using k_{obs} from the plot (c): 7.9 ± 1.4 × 10^{-6} s^{-1} (R^2 = 0.964) for AE−Pyr and 8.3 ± 0.4 × 10^{-6} s^{-1} (R^2 = 0.988) for AE−NH_2.

Therefore, these results suggest that the rate of HPOM dissociation most likely depends on the steric and electron-withdrawing properties of the functional group.

UV−vis spectra of **AE−NH_2** and **AE−CH_3** in PBS(1×) at pH 7.4 acquired over 90 h further confirmed the influence of the functional group on the decomposition (Figure 10). Even at a slightly higher pH, **AE−CH_3** remained largely stable as λ_{max} was only slightly blue-shifted from 215 to 211 nm after 90 h, while for **AE−NH_2**, the faster decomposition into $[MoO_4]^{2-}$ resulted in a shift toward 208 nm and the appearance of a shoulder peak at 230 nm (Figures 10b; S44). Moreover, after 90 h, the absorbance of the LMCT peak increased by only 2% for **AE−CH_3**, while a 16% increase was observed for **AE−NH_2** in the same time period. Similarly, the increase in the absorbance of the d−d transition peak was much more pronounced for **AE−NH_2** as it initially increased and then began to decrease due to the manganese (III) salt precipitating out of solution, as confirmed by IR spectroscopy (Figure S8). In contrast, for **AE−CH_3**, the peak corresponding to the d−d transition increased more gradually and only started to decrease after around 70 h (Figure 10d). Overall, the data from both UV−vis and ^1H NMR are consistent with the fact that the nature of the functional group on the ligand has a large effect on the stability of the HPOM, which is an important factor to be considered when synthesizing new HPOMs that need to be stable under aqueous conditions.

In addition, some ligands also appear to be susceptible to hydrolysis in the presence of water. Over time, the ^1H NMR spectra of both **AE−Cl** and **AE−Biot** showed the formation of tris(hydroxymethyl)aminomethane ($(HOCH_2)_3CNH_2$) along with free chloroacetic acid and biotin, respectively, indicating hydrolysis of the amide bond (Figures S16−S18). Moreover, hydrolysis was likely catalyzed by $[MoO_4]^{2-}$ formed from the decomposition of the HPOM, in accordance with the previously observed reactivity of this oxoanion toward amide bonds (Figure S17).[48,49] On its own in D_2O, around 21% of the prefunctionalized ligand used to synthesize **AE−Cl** ($(HOCH_2)_3CNHCOCH_2Cl$) was hydrolyzed after 14 days, based on the integration of the peaks due to the $-OCH_2-$ protons in the ^1H NMR spectra. However, for a solution of the ligand in the presence of 3 equiv of $[MoO_4]^{2-}$, both at a comparable concentration to that obtained by the full collapse of **AE−Cl**, the ligand decomposed by 70% in the same amount of time. Therefore, due to the catalytic nature of $[MoO_4]^{2-}$, further decomposition of the ligand can take place. Likewise, **AE−Pyr** was observed to undergo hydrolysis of the ligand itself, in this case via the imine bond, to form the **AE−NH_2** HPOM and pyridinecarbaldehyde immediately upon dissolution in D_2O, which shows a much faster rate of decomposition than for **AE−Cl** and **AE−Biot** (Figure 11b).[50,51] Then, after release of pyridinecarbaldehyde, the **AE−NH_2** left in solution was observed to decompose in the same way as previously discussed, with a similar k_{obs} of 7.9 ± 1.4 × 10^{-6} s^{-1} (Figure 11c). Hence, it appears that, despite being commonly used, the amide and imine bonds in these HPOMs are susceptible to hydrolysis, and therefore, alternative methods may need to be considered for attaching organic moieties if a highly stable HPOM in an aqueous environment is desired. Imine bonds are

https://doi.org/10.1021/acs.inorgchem.1c00511
Inorg. Chem. XXXX, XXX, XXX−XXX

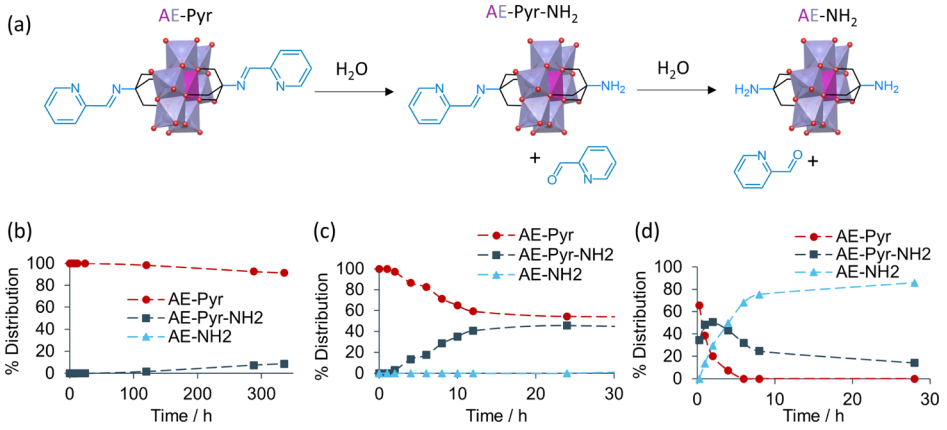

Figure 12. Plots of the changes over time in % distribution of species in solution based on the integration determined by deconvolution of the peaks in the ^{1}H NMR spectra corresponding to the POM-bound $-OCH_2-$ protons due to AE−Pyr and HPOMs formed by (a) the decomposition reaction of AE−Pyr (5 mg/mL) into AE−NH_2, via an asymmetric AE−Pyr−NH_2 HPOM intermediate, in (b) DMSO-d_6 with 15 equiv of residual water, (c) ACN-d_3 with 23 equiv of residual water, and (d) a mixture of 95% ACN-d_3 and 5% D_2O.

Scheme 1. Suggested Mechanism of Decomposition of AE−R in Water by Nucleophilic Attack of Hydroxide Ions at the $-OCH_2-$ Groups Attached to the POM Core, Resulting in the Release of the Free Ligand and Breakdown of the POM Core into Molybdate ($[MoO_4]^{2-}$) and Free Mn^{3+}

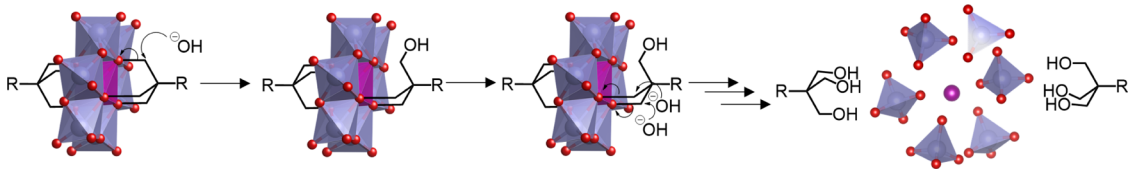

particularly prone to hydrolysis, as full decomposition of **AE−Pyr** into **AE−NH_2** was observed within a few minutes, followed by subsequent decomposition of the resulting **AE−NH_2** in under 1 week. Nevertheless, compared to imine bonds, amide bonds appear to be more stable with only around 25% decomposition observed for **AE−Cl** and **AE−Biot** over 14 days.

Stability in Organic Solvents. The decomposition of these AE−R HPOMs over time was also followed in organic solvents, which showed that the nature of the solvent has a profound influence on the stability of HPOMs. In MeOD-d_4, the appearance of a very weak peak in the range 3.5−4.0 ppm characteristic of the $-OCH_2-$ protons of the free ligand was observed to increase very slowly over time by ^{1}H NMR (Figures S31 and S32), while by UV−vis spectroscopy, the absorbance of **Li−AE−NH_2** in MeOH was observed to slightly decrease over time (Figure S45). However, in ACN, essentially no change was observed in the UV−vis spectra of **TBA−AE−NH_2** as λ_{max} remained constant at 215 nm (Figure S46). Similarly, with the exception of **AE−Pyr**, the ^{1}H NMR spectra of all other HPOMs in DMSO-d_6 and ACN-d_3 remained unchanged over 14 days (Figures S33−S43). As a result, the stability of HPOMs, in general, is much higher in organic solvents and even more so in polar aprotic solvents.

Unlike most other HPOMs, which showed relatively high stability in organic solvents, **AE−Pyr** was highly sensitive to the presence of residual water, which can attack the imine bond to form the **AE−NH_2** HPOM and pyridinecarbaldehyde via an asymmetric **AE−Pyr−NH_2** (δ-$[MnMo_6O_{18}\{(OCH_2)_3$-C−N═CH(2-C_5H_4N)$\}\{(OCH_2)_3C-NH_2\}]^{3-}$) HPOM intermediate (Figure 12).[50] When **AE−Pyr** was dissolved in DMSO-d_6, containing 15 equiv of residual H_2O, it remained relatively stable (Figures 12b; S36) and only started to decompose gradually into pyridinecarbaldehyde and **AE−Pyr−NH_2** after around 5 days. However, in ACN-d_3, which contained a slightly higher amount of residual H_2O (23 equiv), decomposition was much faster (Figures 12c; S41). After only 24 h, 50% of **AE−Pyr** decomposed into **AE−Pyr−NH_2**, and then, the formation of **AE−NH_2** from **AE−Pyr−NH_2** took over as the dominant process. Such a fast decomposition was confirmed to be due to residual water and not ACN itself, as **AE−Pyr** displayed a much faster rate of decomposition in a mixture of 95% ACN-d_3 and 5% D_2O (Figures 12d; S38), with 30% of **AE−Pyr** being converted into **AE−Pyr−NH_2** immediately upon dissolution. Further decomposition into **AE−NH_2** was then observed reaching 100% decomposition of **AE−Pyr** after only 6 h with 75% conversion into **AE−NH_2** after 8 h. As a result, the imine bond seemingly makes HPOMs highly unstable toward hydrolysis and these HPOMs should only be used in highly dry media if high stability is required.[51]

Mechanism of HPOM Decomposition. The observed influence of the chemical nature of the functional group on the tris(alkoxo) ligand, as well as the higher rate of decomposition with increasing pH, suggests that the decomposition mechanism in aqueous solutions occurs via a concerted nucleophilic attack by hydroxide ions at the $-OCH_2-$ groups attached to the POM core. This results in the release of the ligand from the POM and disintegration of the AE POM structure into $[MoO_4]^{2-}$ and free Mn^{3+} as a result (Scheme 1). Electron-withdrawing groups, such as the $-NH_2$ group, will remove electron density from the neighboring $-OCH_2-$ groups, making them more susceptible toward nucleophilic attack. Consequently, the presence of the aliphatic $-CH_3$ group results in a much more stable HPOM. Therefore, placing less-electron-withdrawing groups close to the

https://doi.org/10.1021/acs.inorgchem.1c00511
Inorg. Chem. XXXX, XXX, XXX−XXX

−OCH_2− POM core should be considered for higher stability when synthesizing HPOMs. Furthermore, steric hindrance toward nucleophilic attack at the −OCH_2− groups may also play a role in making HPOMs more stable. The HPOMs with amide bonds, **AE−Cl** and **AE−Biot**, showed intermediate stability, with the bulkier **AE−Biot** displaying a slightly higher stability, which can be due to steric contributions as biotin is known to be able to fold on itself.[52,53] However, although the steric hindrance of the post- and prefunctionalized HPOMs may make them more stable toward decomposition via nucleophilic attack at the −OCH_2− groups, they are susceptible to hydrolysis of the ligand itself, which can be catalyzed by $[MoO_4]^{2-}$ formed upon collapse of the POM. This can lead to further decomposition of the overall structure, depending on the stability of the functional groups linking the ligand to the HPOM. As a result, the chemical structure of the ligand grafted to the HPOM is highly important in determining its stability against decomposition in solution and the nature of the species formed over time.

CONCLUSIONS

The solubility, stability, and speciation under different conditions of several representative HPOMs based on the archetypical AE structure with different functional groups and countercations were established. Since HPOMs are typically synthesized as TBA salts, a cation metathesis procedure was optimized to efficiently obtain full conversion of the HPOMs into the corresponding Li, Na, and K salts in good yields. This fast and efficient procedure resulted in a range of HPOMs with different countercations, which were observed to have a significant effect on the solubility in different solvents. The nature of the ligand also played an important role in the solubility. Therefore, it is possible to tune the solubility of HPOMs through both the counterion and the attached organic moiety.

Once HPOMs were solubilized in aqueous solutions by exchanging the countercation, NMR and UV−vis spectroscopy revealed that the composition of the HPOM and the conditions in solution had a large influence on the stability. In general, the stability of HPOMs significantly decreased with increasing pH and temperature. The dissociation mechanism most likely occurs via a concerted nucleophilic attack by hydroxide ions at the −OCH_2− groups attached to the POM core, resulting in the release of the ligand from the POM and leading to the collapse of the AE structure into $[MoO_4]^{2-}$ and free Mn^{3+}. Although counterions play a key role in solubilizing the HPOM, the presence of different ions in solution did not have a noticeable influence on the stability of HPOMs, allowing for solubility to be altered without affecting stability. However, the nature of the functional group had a large influence on the stability, suggesting that placing less electron-withdrawing and more sterically hindered groups on the quaternary carbon of the tripodal anchor to the POM could favor higher stability. Furthermore, the stability of post-functionalized HPOMs is largely dependent on the type of bond used for postfunctionalization. Ligands bound via amide bonds were shown to undergo hydrolysis, while imine-bound ligands were particularly susceptible to hydrolysis and decomposed even in organic solvents with just traces of water. Consequently, this study gives important insights into the stability of HPOMs, revealing that critical assessment of their solution dynamics is necessary under the conditions of their use. It also highlights the possible strategies that can be applied in the synthesis of new HPOMs, particularly regarding the nature of the functional groups of the ligand and the type of linkage used to attach the ligand to the POM cluster.

ASSOCIATED CONTENT

Supporting Information

The Supporting Information is available free of charge at https://pubs.acs.org/doi/10.1021/acs.inorgchem.1c00511.

Experimental details for the synthesis, cation metathesis, characterization, and stability measurements; approximate solubility tables for all HPOMs; IR, ^{1}H NMR, and UV−vis spectra showing the formation of HPOMs and their stability in solution (PDF)

AUTHOR INFORMATION

Corresponding Author

Tatjana N. Parac-Vogt − *Department of Chemistry, KU Leuven, 3001 Leuven, Belgium*; orcid.org/0000-0002-6188-3957; Email: tatjana.vogt@kuleuven.be

Authors

David E. Salazar Marcano − *Department of Chemistry, KU Leuven, 3001 Leuven, Belgium*

Sarah Lentink − *Department of Chemistry, KU Leuven, 3001 Leuven, Belgium*; orcid.org/0000-0002-4494-3268

Mhamad A. Moussawi − *Department of Chemistry, KU Leuven, 3001 Leuven, Belgium*

Complete contact information is available at: https://pubs.acs.org/10.1021/acs.inorgchem.1c00511

Author Contributions

The manuscript was written through contributions of all authors. All authors have given approval to the final version of the manuscript.

Funding

Research Foundation Flanders (FWO) and KU Leuven.

Notes

The authors declare no competing financial interest.

ACKNOWLEDGMENTS

T.N.P.-V. thanks the Research Foundation Flanders (FWO) and KU Leuven (C14/19/076) for financial support. D.E.S.M. and M.A.M. also thank FWO for PhD (83523/1183021N) and junior postdoctoral (203282/1279721N) fellowships, respectively. We also thank Eirini Tzanetou for her assistance with the synthesis of some of the compounds used in this study. Some of the figures were created with BioRender.com.

REFERENCES

(1) Hutin, M.; Rosnes, M. H.; Long, D.-L.; Cronin, L. Polyoxometalates: Synthesis and Structure - From Building Blocks to Emergent Materials. *Comprehensive Inorganic Chemistry II*; Elsevier, 2013; Vol. 2, pp 241−269.

(2) Blazevic, A.; Rompel, A. The Anderson−Evans polyoxometalate: From inorganic building blocks via hybrid organic−inorganic structures to tomorrows "Bio-POM". *Coord. Chem. Rev.* **2016**, *307*, 42−64.

(3) Patel, A.; Narkhede, N.; Singh, S.; Pathan, S. Keggin-type lacunary and transition metal substituted polyoxometalates as heterogeneous catalysts: A recent progress. *Catal. Rev.* **2016**, *58*, 337−370.

(4) Dolbecq, A.; Dumas, E.; Mayer, C. R.; Mialane, P. Hybrid Organic−Inorganic Polyoxometalate Compounds: From Structural Diversity to Applications. *Chem. Rev.* **2010**, *110*, 6009−6048.
(5) Zhang, J.; Huang, Y.; Li, G.; Wei, Y. Recent advances in alkoxylation chemistry of polyoxometalates: From synthetic strategies, structural overviews to functional applications. *Coord. Chem. Rev.* **2019**, *378*, 395−414.
(6) Anyushin, A. V.; Kondinski, A.; Parac-Vogt, T. N. Hybrid polyoxometalates as post-functionalization platforms: from fundamentals to emerging applications. *Chem. Soc. Rev.* **2020**, *49*, 382.
(7) Proust, A.; Thouvenot, R.; Gouzerh, P. Functionalization of polyoxometalates: towards advanced applications in catalysis and materials science. *Chem. Commun.* **2008**, 1837.
(8) Linnenberg, O.; Kondinski, A.; Monakhov, K. Y. *Supramolecular Systems: Chemistry, Types and Applications*; Nova Science Publishers, 2017; pp. 39−66.
(9) Song, Y.-F.; McMillan, N.; Long, D.-L.; Kane, S.; Malm, J.; Riehle, M. O.; Pradeep, C. P.; Gadegaard, N.; Cronin, L. Micropatterned Surfaces with Covalently Grafted Unsymmetrical Polyoxometalate-Hybrid Clusters Lead to Selective Cell Adhesion. *J. Am. Chem. Soc.* **2009**, *131*, 1340−1341.
(10) Martin, C.; Kastner, K.; Cameron, J. M.; Hampson, E.; Alves Fernandes, J.; Gibson, E. K.; Walsh, D. A.; Sans, V.; Newton, G. N. Redox-Active Hybrid Polyoxometalate-Stabilised Gold Nanoparticles. *Angew. Chem., Int. Ed.* **2020**, *59*, 14331−14335.
(11) Yan, J.; Zheng, X.; Yao, J.; Xu, P.; Miao, Z.; Li, J.; Lv, Z.; Zhang, Q.; Yan, Y. Metallopolymers from organically modified polyoxometalates (MOMPs): A review. *J. Organomet. Chem.* **2019**, *884*, 1−16.
(12) Diab, M.; Mateo, A.; Al Cheikh, J.; Haouas, M.; Ranjbari, A.; Bourdreux, F.; Naoufal, D.; Cadot, E.; Bo, C.; Floquet, S. Unprecedented coupling reaction between two anionic species of a closo-decahydrodecaborate cluster and an Anderson-type polyoxometalate. *Dalton Trans.* **2020**, *49*, 4685−4689.
(13) Hu, M.-B.; Hou, Z.-Y.; Hao, W.-Q.; Xiao, Y.; Yu, W.; Ma, C.; Ren, L.-J.; Zheng, P.; Wang, W. POM-Organic-POSS Cocluster: Creating A Dumbbell-Shaped Hybrid Molecule for Programming Hierarchical Supramolecular Nanostructures. *Langmuir* **2013**, *29*, 5714−5722.
(14) Zhang, J.; Hao, J.; Wei, Y.; Xiao, F.; Yin, P.; Wang, L. Nanoscale Chiral Rod-like Molecular Triads Assembled from Achiral Polyoxometalates. *J. Am. Chem. Soc.* **2010**, *132*, 14−15.
(15) Kastner, K.; Kibler, A. J.; Karjalainen, E.; Fernandes, J. A.; Sans, V.; Newton, G. N. Redox-active organic-inorganic hybrid polyoxometalate micelles. *J. Mater. Chem. A* **2017**, *5*, 11577−11581.
(16) Pradeep, C. P.; Misdrahi, M. F.; Li, F.-Y.; Zhang, J.; Xu, L.; Long, D.-L.; Liu, T.; Cronin, L. Synthesis of Modular "Inorganic-Organic-Inorganic" Polyoxometalates and Their Assembly into Vesicles. *Angew. Chem.* **2009**, *121*, 8459−8463.
(17) Li, D.; Song, J.; Yin, P.; Simotwo, S.; Bassler, A. J.; Aung, Y.; Roberts, J. E.; Hardcastle, K. I.; Hill, C. L.; Liu, T. Inorganic-organic hybrid vesicles with counterion- and pH-controlled fluorescent properties. *J. Am. Chem. Soc.* **2011**, *133*, 14010−14016.
(18) Tong, U.; Chen, W.; Ritchie, C.; Wang, X.; Song, Y.-F. Reversible Light-Driven Polymerization of Polyoxometalate Tethered with Coumarin Molecules. *Chem.—Eur. J.* **2014**, *20*, 1500−1504.
(19) Sullivan, K. P.; Neiwert, W. A.; Zeng, H.; Mehta, A. K.; Yin, Q.; Hillesheim, D. A.; Vivek, S.; Yin, P.; Collins-Wildman, D. L.; Weeks, E. R.; Liu, T.; Hill, C. L. Polyoxometalate-based gelating networks for entrapment and catalytic decontamination. *Chem. Commun.* **2017**, *53*, 11480−11483.
(20) He, Z.; Li, B.; Ai, H.; Li, H.; Wu, L. A processable hybrid supramolecular polymer formed by base pair modified polyoxometalate clusters. *Chem. Commun.* **2013**, *49*, 8039.
(21) Saad, A.; Oms, O.; Marrot, J.; Dolbecq, A.; Hakouk, K.; El Bekkachi, H.; Jobic, S.; Deniard, P.; Dessapt, R.; Garrot, D.; Boukheddaden, K.; Liu, R.; Zhang, G.; Keita, B.; Mialane, P. Design and optical investigations of a spironaphthoxazine/polyoxometalate/spiropyran triad. *J. Mater. Chem. C* **2014**, *2*, 4748−4758.
(22) Oms, O.; Hakouk, K.; Dessapt, R.; Deniard, P.; Jobic, S.; Dolbecq, A.; Palacin, T.; Nadjo, L.; Keita, B.; Marrot, J.; Mialane, P. Photo- and electrochromic properties of covalently connected symmetrical and unsymmetrical spiropyran-polyoxometalate dyads. *Chem. Commun.* **2012**, *48*, 12103−12105.
(23) Bijelic, A.; Aureliano, M.; Rompel, A. Polyoxometalates as Potential Next-Generation Metallodrugs in the Combat Against Cancer. *Angew. Chem., Int. Ed.* **2019**, *58*, 2980−2999.
(24) Bijelic, A.; Aureliano, M.; Rompel, A. The antibacterial activity of polyoxometalates: structures, antibiotic effects and future perspectives. *Chem. Commun.* **2018**, *54*, 1153−1169.
(25) Bijelic, A.; Rompel, A. Polyoxometalates: more than a phasing tool in protein crystallography. *ChemTexts* **2018**, *4*, 10.
(26) Proust, A.; Matt, B.; Villanneau, R.; Guillemot, G.; Gouzerh, P.; Izzet, G. Functionalization and post-functionalization: a step towards polyoxometalate-based materials. *Chem. Soc. Rev.* **2012**, *41*, 7605.
(27) Yang, H.-K.; Zhao, H.; Wang, X.-M.; Li, Y.-K. A survey of the influence of EEDQ on efficient post-functionalization of an Anderson-type polyoxomolybdate towards construction of organic-inorganic hybrids. *Colloids Surf., A* **2018**, *538*, 711−719.
(28) Vanhaecht, S.; Quanten, T.; Parac-Vogt, T. N. A Simple Nucleophilic Substitution as a Versatile Postfunctionalization Method for the Coupling of Nucleophiles to an Anderson-Type Polyoxometalate. *Inorg. Chem.* **2017**, *56*, 3095−3101.
(29) Vanhaecht, S.; Jacobs, J.; Van Meervelt, L.; Parac-Vogt, T. N. A versatile and highly efficient post-functionalization method for grafting organic molecules onto Anderson-type polyoxometalates. *Dalton Trans.* **2015**, *44*, 19059−19062.
(30) Ventura, D.; Calderan, A.; Honisch, C.; Krol, S.; Serratì, S.; Bonchio, M.; Carraro, M.; Ruzza, P. Synthesis and biological activity of anAnderson polyoxometalate bis-functionalized with aBombesin-analog peptide. *Pept. Sci.* **2018**, *110*, No. e24047.
(31) Zhang, C.; Lin, X.; Zhang, Z.; Long, L.-S.; Wang, C.; Lin, W. A hybrid polyoxometalate-organic molecular catalyst for visible light driven water oxidation. *Chem. Commun.* **2014**, *50*, 11591−11594.
(32) Berardi, S.; Carraro, M.; Sartorel, A.; Modugno, G.; Bonchio, M. Hybrid Polyoxometalates: Merging Organic and Inorganic Domains for Enhanced Catalysis and Energy Applications. *Isr. J. Chem.* **2011**, *51*, 259−274.
(33) Misra, A.; Kozma, K.; Streb, C.; Nyman, M. Beyond Charge Balance: Counter-Cations in Polyoxometalate Chemistry. *Angew. Chem., Int. Ed.* **2020**, *59*, 596−612.
(34) Al-Sayed, E.; Blazevic, A.; Roller, A.; Rompel, A. The Synthesis and Characterization of Aromatic Hybrid Anderson-Evans POMs and their Serum Albumin Interactions: The Shift from Polar to Hydrophobic Interactions. *Chem.—Eur. J.* **2015**, *21*, 17800−17807.
(35) Zhang, B.; Yue, L.; Wang, Y.; Yang, Y.; Wu, L. A novel single-side azobenzene-grafted Anderson-type polyoxometalate for recognition-induced chiral migration. *Chem. Commun.* **2014**, *50*, 10823−10826.
(36) Vandebroek, L.; De Zitter, E.; Ly, H. G. T.; Conić, D.; Mihaylov, T.; Sap, A.; Proost, P.; Pierloot, K.; Van Meervelt, L.; Parac-Vogt, T. N. Protein-Assisted Formation and Stabilization of Catalytically Active Polyoxometalate Species. *Chem.—Eur. J.* **2018**, *24*, 10099−10108.
(37) Gao, D.; Trentin, I.; Schwiedrzik, L.; González, L.; Streb, C. The Reactivity and Stability of Polyoxometalate Water Oxidation Electrocatalysts. *Molecules* **2019**, *25*, 157.
(38) Gumerova, N. I.; Rompel, A. Polyoxometalates in solution: speciation under spotlight. *Chem. Soc. Rev.* **2020**, *49*, 7568−7601.
(39) Wilson, E. F.; Miras, H. N.; Rosnes, M. H.; Cronin, L. Real-Time Observation of the Self-Assembly of Hybrid Polyoxometalates Using Mass Spectrometry. *Angew. Chem., Int. Ed.* **2011**, *50*, 3720−3724.
(40) Blazevic, A.; Al-Sayed, E.; Roller, A.; Giester, G.; Rompel, A. Tris-Functionalized Hybrid Anderson Polyoxometalates: Synthesis, Characterization, Hydrolytic Stability and Inversion of Protein Surface Charge. *Chem.—Eur. J.* **2015**, *21*, 4762−4771.

https://doi.org/10.1021/acs.inorgchem.1c00511
Inorg. Chem. XXXX, XXX, XXX−XXX

(41) Bijelic, A.; Dobrov, A.; Roller, A.; Rompel, A. Binding of a Fatty Acid-Functionalized Anderson-Type Polyoxometalate to Human Serum Albumin. *Inorg. Chem.* **2020**, *59*, 5243−5246.
(42) Yamase, T. Anti-tumor, -viral, and -bacterial activities of polyoxometalates for realizing an inorganic drug. *J. Mater. Chem.* **2005**, *15*, 4773.
(43) Marcoux, P. R.; Hasenknopf, B.; Vaissermann, J.; Gouzerh, P. Developing Remote Metal Binding Sites in Heteropolymolybdates. *Eur. J. Inorg. Chem.* **2003**, 2406−2412.
(44) Hasenknopf, B.; Delmont, R.; Herson, P.; Gouzerh, P. Anderson-Type Heteropolymolybdates Containing Tris(alkoxo) Ligands: Synthesis and Structural Characterization. *Eur. J. Inorg. Chem.* **2002**, 1081−1087.
(45) Zhang, J.; Huang, Y.; Zhang, J.; She, S.; Hao, J.; Wei, Y. A direct anchoring of Anderson-type polyoxometalates in aqueous media with tripodal ligands especially containing the carboxyl group. *Dalton Trans.* **2014**, *43*, 2722−2725.
(46) Hakouk, K.; Oms, O.; Dolbecq, A.; Marrot, J.; Saad, A.; Mialane, P.; El Bekkachi, H.; Jobic, S.; Deniard, P.; Dessapt, R. New photoresponsive charge-transfer spiropyran/polyoxometalate assemblies with highly tunable optical properties. *J. Mater. Chem. C* **2014**, *2*, 1628.
(47) Ozeki, T.; Kihara, H.; Ikeda, S. Study of equilibria in 0.03 mM molybdate acidic aqueous solutions by factor analysis applied to ultraviolet spectra. *Anal. Chem.* **1988**, *60*, 2055−2059.
(48) Ho, P. H.; Stroobants, K.; Parac-Vogt, T. N. Hydrolysis of Serine-Containing Peptides at Neutral pH Promoted by [MoO4]2- Oxyanion. *Inorg. Chem.* **2011**, *50*, 12025−12033.
(49) Stroobants, K.; Ho, P. H.; Moelants, E.; Proost, P.; Parac-Vogt, T. N. Selective hydrolysis of hen egg white lysozyme at Asp-X peptide bonds promoted by oxomolybdate. *J. Inorg. Biochem.* **2014**, *136*, 73−80.
(50) Cordes, E. H.; Jencks, W. P. On the Mechanism of Schiff Base Formation and Hydrolysis. *J. Am. Chem. Soc.* **1962**, *84*, 832−837.
(51) Schönweiz, S.; Rommel, S. A.; Kübel, J.; Micheel, M.; Dietzek, B.; Rau, S.; Streb, C. Covalent Photosensitizer-Polyoxometalate-Catalyst Dyads for Visible-Light-Driven Hydrogen Evolution. *Chem.—Eur. J.* **2016**, *22*, 12002−12005.
(52) Lei, Y.; Li, H.; Zhang, R.; Han, S. Molecular Dynamics Simulations of Biotin in Aqueous Solution. *J. Phys. Chem. B* **2004**, *108*, 10131−10137.
(53) Strzelczyk, A. A.; Dobrowolski, J. C.; Mazurek, A. P. On the conformation of the biotin molecule. *J. Mol. Struct.: THEOCHEM* **2001**, *541*, 283−290.

https://doi.org/10.1021/acs.inorgchem.1c00511
Inorg. Chem. XXXX, XXX, XXX−XXX